at least close to degeneracy, i.e. the wavelength of both photons of the pair is identical. A subsequent spatial splitting of the pair has been applied using a standard 50:50 beam splitter or a fiber coupler. This has a severe drawback because only half of the generated pairs are spatially separated. This does not only reduce the effective generation efficiency, but also necessitates a post-selection process for the extraction of the entanglement which prohibits many applications like e.g. entanglement distillation (see e.g. [11]).

To overcome this drawback, a nondegenerate PDC scheme exploiting a biperiodic poling structure has been proposed [12]. The biperiodic poling enables simultaneous type II phase-matching for two PDC-processes. The poling periods must be chosen that in the first process a pair with a TE-polarized photon at λ_1 and a TM-polarized photon at λ_2 and in the second process a pair at the same wavelengths but opposite polarization is generated.

The practical implementation of such a scheme has been demonstrated in previous work. In [9] a PPLN waveguide is used with one fixed poling period. To obtain phase-matching for two (slightly) different processes, one part of the sample was covered with a dielectric overlay resulting in a shift of the propagation constants of the guided modes. In [13] a bulk optical PPLN crystal with a biperiodic poling structure consisting of a first section with poling period $\Lambda_1 = 9.25\mu$m and a second section with $\Lambda_2 = 9.5\mu$m has been used to generate the polarization entangled pairs. Both approaches used a *sequential* arrangement, i.e. the first PDC process occurs in a first section followed by a further section for the second PDC process. In this way the processes are spatially separated with the disadvantage that any imbalance can lead to a remaining distinguishabilty and, thus, deteriorates the quality of entanglement.

An advanced approach exploits the whole interaction length for both processes [14, 15]. This scheme applies *interlaced* sections of different poling periods to obtain enhanced indistinguishability. Any variation of process parameters, e.g. pump depletion due to waveguide losses, will simultaneously effect both processes and, thus, preserves the indistinguishability. In this paper we present an integrated source exploiting this scheme. Our source, which provides polarization entangled pairs in the telecom regime, essentially consists of a PPLN waveguide with a specifically tailored ferroelectric domain pattern for the generation of photon pairs in combination with standard fiber optical components.

The paper is structured as follows: In the next section we discuss the principle of operation followed by a discussion of the design, fabrication and classical characterization of the integrated optical chip in Sec.3. Details of the entire entangled source and its performance are given in Sec.4.

2. Principle of operation

The basic principle of our entangled photon pair source relies on the generation of photon pairs by PDC in a periodically poled lithium niobate waveguide. In a PDC process, a pump photon decays into a photon pair, typically labeled as signal and idler photons. We generate orthogonally polarized photon pairs by applying a type II phase-matched PDC process which exploits the non-linear coefficient d_{31} instead of the frequently used type I process. This uses the larger d_{33} coefficient, but provides only extraordinarily polarized photons. Besides energy conservation (quasi-)phase-matching is required for an efficient process (see e.g. [16]):

$$\beta_p = \beta_s + \beta_i + \frac{2\pi}{\Lambda} \tag{1}$$

with β_j $(j = p,s,i)$ being the wave numbers of the pump, signal and idler wave, respectively. The parameter Λ is the period of the ferroelectric domain pattern.

In Fig. 1 calculated phase-matching characteristics of our type II process are shown, where the signal and idler wavelengths are plotted as function of the pump wavelength for two different poling periods $\Lambda_1 = 9.30$ μm (solid lines) and $\Lambda_2 = 9.37$ μm (dashed lines). For a fixed

#194865 - $15.00 USD Received 29 Jul 2013; revised 20 Sep 2013; accepted 21 Sep 2013; published 7 Nov 2013

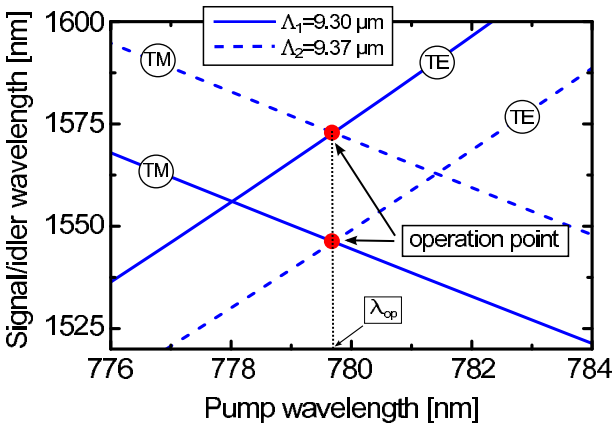

Fig. 1. Calculated phase-matching characteristics of type II phase-matched PDC processes in a PPLN waveguide assuming a poling period of $\Lambda_1 = 9.30\ \mu$m (solid lines) and $\Lambda_2 = 9.37\ \mu$m (dashed curves), respectively. The operation point for the generation of polarization entangled pairs is at the intersection of the phase-matching characteristics of the two periodicities.

single poling period the curves have a cross-like shape. Thus, at the intersection of the curve wavelength degenerate photon pairs can be generated. But, as pointed out in the introduction, polarization entangled pairs can only be generated with a beam splitter followed by a post-selection process.

With a biperiodic pattern, non-degenerate polarization-entangled pairs can directly be generated: The Ti:PPLN waveguide is poled with two periodicities Λ_1 and Λ_2, such that the photon pairs can be generated by two different PDC processes, one corresponding to Λ_1 and the other to Λ_2. Polarization entangled pairs are obtained if the device is operated at a pump wavelength where the TE emission of Λ_1 coincides with the TM emission of Λ_2 and vice versa (see Fig. 1). The generated state is then given by:

$$|\psi\rangle = \frac{1}{\sqrt{2}}\left[|H\rangle_{\lambda_s}|V\rangle_{\lambda_i} + e^{i\Phi}|V\rangle_{\lambda_s}|H\rangle_{\lambda_i}\right] \tag{2}$$

with λ_s and λ_i being the wavelength of the signal and idler photons, respectively. The states $|H\rangle$ and $|V\rangle$ represent TE and TM polarized single photon states, respectively, and Φ is the relative phase between the photon pairs emerging from the waveguide.

This generation scheme can be implemented using a sequential arrangement of sections with two different poling periods, i.e. a first section of poling period Λ_1 is followed by a second section with Λ_2. These two sections must be perfectly balanced exhibiting the same PDC properties (efficiency, bandwidth, ...) for high quality entanglement. Practically, however, an imbalance can be hardly avoided. For instance, waveguide losses cause a depletion of the pump power along the waveguide resulting in a weaker pumping in the second section. To overcome this problem a homogeneous distribution of the two PDC processes along the entire waveguide structure is required. Using the overall waveguide length for the two processes provides also a further advantage: The spectral bandwidth of the generated photons scales reciprocal with length, thus, the predicted PDC bandwidth is significantly smaller because the entire poled area is used for both processes.

To approximate such a homogeneous distribution over the whole waveguide length, our implementation uses an *interlaced* scheme which consists of a sequence of short sections with

#194865 - $15.00 USD Received 29 Jul 2013; revised 20 Sep 2013; accepted 21 Sep 2013; published 7 Nov 2013

alternating poling periods. Details of the practical implementation of this scheme will be given in the following section.

A crucial demand to obtain high quality entanglement is to erase any residual temporal distinguishabiltiy of the two generation processes. The birefringence of the PPLN waveguides results in a differential group delay $\Delta\tau = (n_{go} - n_{ge})L/c$ between TE- and TM-polarized photons with n_{ge} and n_{go} being the respective group refractive indices and L the propagation length within the birefringent waveguide. Due to the larger group velocity of extra-ordinary polarized TM photons, these photons travel faster through the waveguide. A common means to "erase" this distinguishability is using a compensating crystal behind the PDC source which provides a negative group delay of $\Delta\tau_c = -\Delta\tau/2$ (see e.g. [1, 7]). However, applying this scheme to the non-degenerate source with a *sequential* arrangement consisting of two sections with a length of L_1 and L_2, respectively, results in an incomplete compensation: The photon pairs, which are generated in the first section, obtain a further temporal separation when they pass the second section. Thus, compensation for the first section would require $\Delta\tau_c = -(n_{ge}(\lambda_s) - n_{go}(\lambda_i))(L_1/2 + L_2)/c)$, whereas the photon pairs, which are generated in the second section, require a compensation of $\Delta\tau_c = -(n_{ge}(\lambda_i) - n_{go}(\lambda_s))(L_2/2)/c)$. Obviously, both conditions cannot be fulfilled simultaneously with one crystal. On the contrary, using the *interlaced* scheme, an almost perfect compensation can be obtained. Because the two processes are equally distributed over the entire interaction length L the compensation requires for both processes almost the same $\Delta\tau_c$. Only a slight residual difference is left arising from the group velocity dispersion, i.e. $n_{ge}(\lambda_i) - n_{go}(\lambda_s)$ and $n_{ge}(\lambda_s) - n_{go}(\lambda_i))$ differ slightly. However, as long as the wavelength separation between λ_s and λ_i is small, the impact can be neglected.

3. PDC waveguide source

3.1. Waveguide design and fabrication

The detailed structure of the integrated optical PDC source is shown schematically in Fig. 2. The 60 mm long waveguide was fabricated by an indiffusion of a 90 nm thick Ti-stripe into the 0.5 mm thick Z-cut $LiNbO_3$ substrate at 1060 ^{o}C for 9 h. The stripe width in the interaction region is 7 μm. This fabrication process provides single mode waveguides in the telecom range for both polarizations with typical waveguide losses of about 0.1 dB/cm. For the pump wave at $\lambda \approx 780$ nm the waveguide is multi-mode. To improve the coupling into the fundamental mode, a taper region is used in which the stripe width increases linearly from about 3 μm to 7 μm over 10 mm length.

Subsequent to waveguide fabrication, the periodic poling was done by field assisted domain inversion. The poling pattern is engineered to provide the interlaced structure: A first section with N domain periods with periodicity $\Lambda_1 = 9.30$ μm is followed by a similar section with periodicity $\Lambda_2 = 9.37$ μm. This sequence is repeated over the whole 50 mm interaction length.

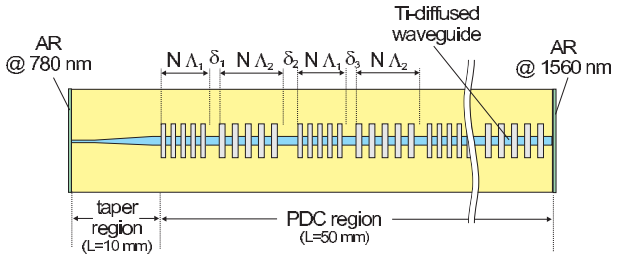

Fig. 2. Detailed design of the integrated PDC source with interlaced poling pattern.

#194865 - $15.00 USD Received 29 Jul 2013; revised 20 Sep 2013; accepted 21 Sep 2013; published 7 Nov 2013

The spacings δ_i between the different sections are chosen in a way that the overall spacing between sections with the same periodicity is a respective integer multiple of this periodicity. We have investigated different structures with $N = 10, 100, 500$ of domain periods per section. Finally, we selected the one with the smallest number of domains, i.e. $N = 10$, because this provided the largest separation of satellite peaks as will be discussed in Sec. 3.2.

After polishing the end-faces AR coatings were deposited. They consist of single quarter-wave layers of SiO_2 to mimize reflection loss of the pump at the input and of the generated PDC photons at the output. The transmission (measured using a witness sample) is $T \approx 95\%$ for the pump at the input face and $T > 96$ % for signal and idler at the output face.

3.2. Classical characterization

As a first step we set up an experiment to test and characterize the integrated PPLN sample by means of second harmonic (SH) generation. For this purpose, light from an extended cavity laser (ECL) tunable in the telecom regime was coupled into the waveguide. A linear input polarization at 45^o was chosen to excite TE and TM waveguide modes simultaneously. Fig. 3 shows the measured SH power as function of the ECL wavelength. Within the scanned wavelength range three pairs of peaks can be recognized. The dominant pair is the wanted one due to SH generation of the fundamental modes in the sections with Λ_1 and Λ_2 periodicities, respectively. The pair in the middle of the spectrum is caused by SH generation resulting from a coupling between the fundamental waveguide modes (TE_{00} and TM_{00}) to the higher mode TE_{20} at the SH wavelength. The additional pair at the shortest wavelength - and a similar pair on the long wavelength side outside of the measurement window - are satellite peaks arising from the segmentation of the poling pattern. These satellites occur because the regular interlacing of segments with different poling periodicities results in a QPM superlattice providing additional wave vectors for phase-matching.

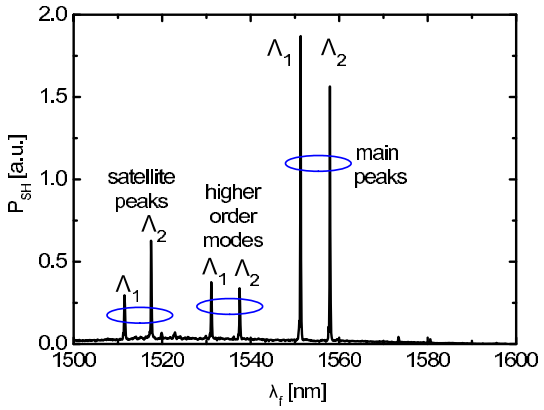

Fig. 3. Measured second harmonic power versus wavelength of the fundamental wave. Details are described in the text.

From our SH measurements we determine a conversion efficiency $\eta_{SH} = P_{SH}/(P_{TE} \times P_{TM}) \approx 0.7\ \%/W$, where P_{SH}, P_{TE}, P_{TM} denote the power of the generated SH wave and the power of the fundamental mode in TE- and TM-polarization, respectively. Using this SH efficiency, the efficiency of the PDC process, defined by the ratio of the generated PDC photon pairs to the number of pump photons, can be estimated to be $\eta_{PDC} \approx 1.4 \times 10^{-10}$ according to the model described in [17].

In the second step we performed a characterization by PDC to investigate the phase-matching and spectral properties of the source. The waveguide was pumped with 200 ns long pulses

#194865 - $15.00 USD Received 29 Jul 2013; revised 20 Sep 2013; accepted 21 Sep 2013; published 7 Nov 2013

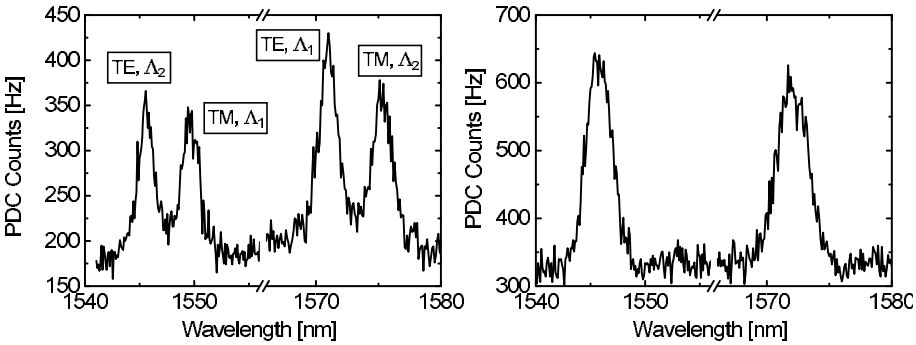

Fig. 4. Results of spectrally resolved PDC measurements with $\lambda_p = 780.0$ nm. Left: PDC spectrum at a sample temperature of $T = 159.2\ ^oC$ resulting in separated spectral peaks. Right: Same measurement at $T = 156.4\ ^oC$ indicating the correct operation point for polarization entanglement.

at $\lambda_p = 780.0$ nm, which were extracted from an external cavity laser (Toptica DL Pro) by an acoustooptical modulator. After a blocking filter suppressing the pump wave, the photons were launched into a fiber coupled acoustooptical tunable filter with a spectral resolution of $\approx$1.5 nm [18] and subsequently detected with an InGaAs-single photon detection module (idQuantique 201). The waveguide was temperature stabilized at temperatures around 160 ^{o}C (with 0.1 ^{o}C stability) to prevent optical damage due to photorefraction.

In Fig. 4 two measured spectra are shown. The measurement yielding the results presented on the left has been performed at a sample temperature of $T = 159.2\ ^oC$. Four distinct peaks are observable, which correspond from left to right to TE-polarized photons generated in the PDC section with period Λ_2, TM-polarized from section Λ_1, TE-polarized from section Λ_1 and TM-polarized from section Λ_2. (The polarizations could be confirmed by inserting an additional polarizer with the appropriate transmission behind the waveguide.) To reach the operation point for polarization entanglement the sample temperature has been lowered to $T = 156.4\ ^oC$. At this temperature the corresponding two peaks overlap completely as illustrated in the right diagram of Fig. 4.

The spectral width of the measured curves is about 1.6 nm; but this is essentially determined by the resolution of the acoustooptical filter ($\approx$ 1.5 nm). Thus, the spectral bandwidth of the generated PDC signals is not directly measurable with this method. Therefore, we employed difference frequency generation (DFG) to obtain detailed information on the spectral structure. For this purpose the light from an ECL - tunable around $\lambda = 1550$ nm - was superimposed to the pump beam. The generated DFG signal was recorded as function of the ECL wavelength as shown in Fig. 5. By setting the input polarization either to TE or TM the conversions belonging to the two different processes could be investigated separately. We found that the shape of the central peak fits quite well and the spectral width (FWHM) is about 0.7 nm. This value is only slightly larger than the theoretically predicted bandwidth of 0.58 nm for a source with 50 mm interaction length. However, we observed more pronounced sidelobes than expected. The deviation from the ideal spectral shape can probably be explained by inhomogeneities of the waveguide along the interaction length. Unfortunately, the shapes of sidelobes of the two curves are different which impact the quality of entanglement as will be discussed in the next section.

In the next step we studied the efficiency of the generation process by using correlation measurements. The generated photons pairs were coupled into a fiber WDM-coupler, spatially separated and detected by single photon detectors. The timing of the registered counting events

#194865 - $15.00 USD Received 29 Jul 2013; revised 20 Sep 2013; accepted 21 Sep 2013; published 7 Nov 2013

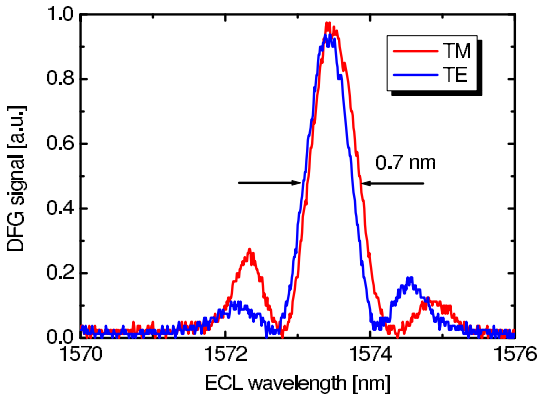

Fig. 5. Measured difference frequency power as function of the wavelength of the ECL acting as signal source for the DFG process. By setting the input polarization either to TE or TM, the two different nonlinear process can be probed separately.

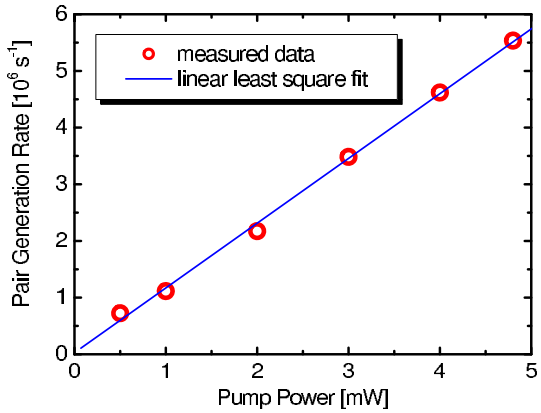

Fig. 6. Photon pair generation rate (determined from coincidence measurement) versus pump power. The symbols show the measured data, the solid line is a linear least square fit.

was then analyzed with a time-to-digital converter. We determined the PDC efficiency from the ratio of the coincidence events to the single counts. Fig. 6 presents the measured pair generation rate in dependence of the pump power, which was measured in front of the waveguide. The curve shows a linear relation as predicted. From the slope of this curve a PDC efficiency of $\eta_{PDC} = 3 \times 10^{-10}$ is obtained, which is in reasonable good agreement with the predicted efficiency derived from the SH experiments. From this value in combination with the width of the measured spectra a brightness of $B \approx 7 \times 10^3$ pairs/(s$\times$mW$\times$GHz) can be estimated for our source.

4. Entanglement

4.1. Source implementation and characterization

After the basic characterization of our waveguide structure, we set up an experiment for the implementation and characterization of the complete entanglement source. In Fig. 7 the overall configuration is shown. The spatial splitting behind the integrated PDC source is accomplished using a fiber 1x4 wavelength division demultiplexer (cWDM), which is a standard component

#194865 - $15.00 USD Received 29 Jul 2013; revised 20 Sep 2013; accepted 21 Sep 2013; published 7 Nov 2013

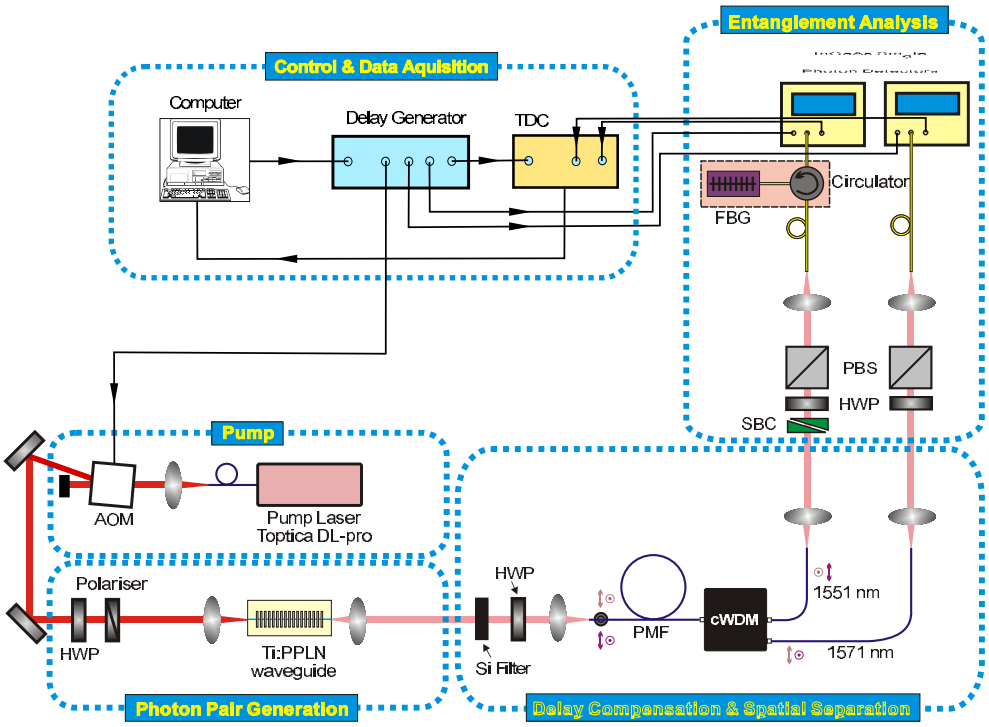

Fig. 7. Experimental setup for the investigation of entanglement. (TDC: time-to-digital converter; AOM: acoustooptical modulator; HWP: half-wave retardation plate; PMF: polarisation-maintaining fiber; cWDM: coarse WDM fiber demultiplexer; SBC: Soleil-Babinet compensator; PBS: polarisation beam splitter; FBG: fiber Bragg grating).

of telecom fiber networks originally dedicated for coarse WDM applications. We used two output ports centered around 1551 nm and 1571 nm, respectively, with a passband width of 13 nm. The entire cWDM coupler (with specified insertion loss < 2 dB) is equipped with polarization maintaining fibers (PMF).

As discussed in Sec. 2, the residual temporal distinguishability of the two generation processes must be compensated. For the 50 mm long interaction length we estimated that a delay of ≈ 6.2 ps is required for temporal compensation. Note that the difference for the optimum compensation for the two processes arising from group velocity dispersion is only about 0.1 ps. Instead of using a further birefringent crystal for the compensation, we used a polarization maintaining fiber (PMF), which was aligned to couple TE(TM)-polarized photons into the fast (slow) axis mode. This fiber was directly spliced to the input fiber of the CWDM coupler. The coupler generates an additional group delay which had to be taken into account to determine the optimum length of the PMF. The length of the PMF was successively cut until the optimum compensation could be achieved.

We characterized the entanglement using two rotatable half-wave plates (HWPs) in front of polarization splitters (PBS). A Soleil Babinet compensators (SBC) in one analysis arm enables a fine tuning of the phase Φ. Behind the PBS the photons are coupled into single mode fibers and routed to single photon detectors (idQuantique id201). The detection events (at t_s and t_i from the signal and idler photons) are temporally resolved recorded via a time-to-digital converter enabling the evaluation of joint arrival time statistics. Mainly the temporal jitter of the detectors (< 800 ps) limits the temporal resolution. We evaluated the coincidences by selecting all events

#194865 - $15.00 USD Received 29 Jul 2013; revised 20 Sep 2013; accepted 21 Sep 2013; published 7 Nov 2013

with $|t_s - t_i| \leq 2$ ns. The raw data, i.e. the number of coincidence events in the coincidence window, were corrected by substracting the accidental events. These were determined from the measured number of coincidence counts outside of the coincidence window. This procedure does not correct for multi-photon events.

4.2. Results and discussion

We performed correlation measurements at various settings of the HWPs. From the measured coincidence counts we determined the net visibilities. In the first experiments we found that the initial visibilities in the H/V- and the D/A-bases were only around 70 % (see Fig. 8, left).

One reason for this relatively low visibility could be attributed to the different spectral shapes of the two processes as revealed by the DFG measurements (Fig. 5). The different spectral distributions (in particular in the sidelobes) as well as the associated phases, which cannot be extracted from the DFG signals, lead to a reduced indistinguishability and, thus, caused the reduced visibility. To overcome this problem we inserted an additional bandpass filter consisting of a fiber Bragg grating and a circulator (see Fig. 7) in one of the analysis arms. The FWHM of this filter was about 0.5 nm and, thus, matched exactly the width of the main lobe of the PDC processes. With this filter in place the visibility increased to above 90%.

The remaining limitation of the visibility can mostly be explained by multiphoton pair generation. Launching 16 mW pump power into the waveguide results in a highly efficient PDC generation with a high probability to generate multiple pairs. The calculated mean photon number within the 4 ns wide coincidence window is $\alpha \approx 0.08$. Following the model on the impact of multiphoton effects on the visibility described in [19] a maximum visibility of about 92.5% can be expected.

Reducing the pump power to 6 mW and, thus, the mean photon number in a coincidence window to $\alpha \approx 0.03$, increased significantly the visibility. A typical measurement result is shown in the right diagram of Fig. 8. A net visibility of more than 95% has been obtained at the reduced pump power. This result highlights that for all applications of the source a certain trade-off between generation rate and visibility must be selected.

The final limitation concerning the visibility actually arose from losses within the entire system and a residual polarization dependence of these losses. The measured overall transmisson from the waveguide output facet to the single photon detectors was only about 15 %. Most of these losses arose from the incoupling into the fibers, fiber splice losses and the intrinsic losses

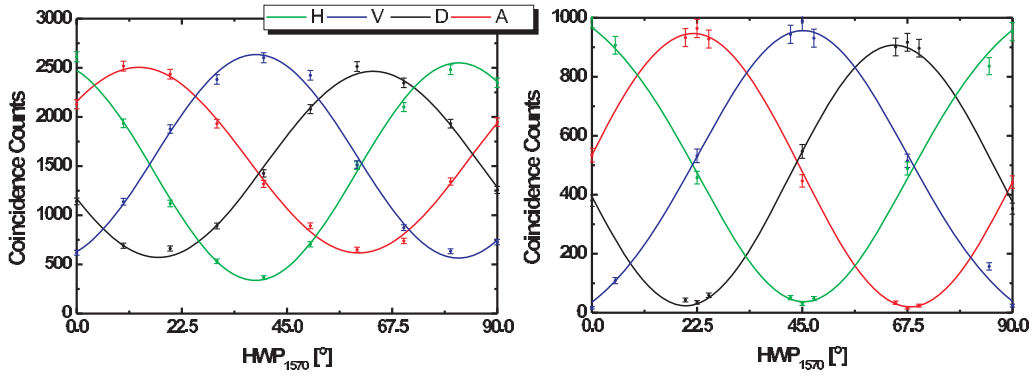

Fig. 8. Measured visibilities of the entangled photon pair source in the various bases: Left: Visibilities without the additional bandpass filter in the analysis arm and at an input pump power of 16 mW; right: visibilities with additional bandpass filter and input pump power of 6 mW.

#194865 - $15.00 USD Received 29 Jul 2013; revised 20 Sep 2013; accepted 21 Sep 2013; published 7 Nov 2013

of the commercial cWDM. Due to all these losses a further reduction of the pump power was not possible to determine the ultimate limit of the visibility because at lower pump powers the count rates dropped below the dark counts preventing a reliable measurement.

An important benchmark of the performance of our entangled source provides the testing of the violation of the Bell inequality. From our measurements we could extract the coincidence data for the various HWP settings required to perform the CHSH test [20] which enabled us to determine the *S*-parameter to be $S = 2.57 \pm 0.06$. This is a violation of the Bell inequality by more than 9 standards deviations indicating the generation of strongly non-classical photon pairs.

5. Conclusions

We have demonstrated a new source providing polarization-entangled photon-pairs in the telecom regime. Highly efficient photon pair generation is obtained employing PDC in a Ti-diffused PPLN waveguide with an interlaced bi-periodic ferroelectric domain pattern which facilitates type II phase-matching for two wavelength combinations. In combination with standard fiber optical components non-degenerated polarization entangled photon pairs are generated in a fully integrated setup.

A brightness of the waveguide PDC source as high as $B \approx 7 \times 10^3$ pairs/(s$\times$mW$\times$GHz) could be demonstrated. Our measured visibilities of up to 95% were mainly limited by residual losses in the source and the measurement system. The excellent source characteristics are also verified by the violation of the Bell inequality with $S = 2.57 \pm 0.06$.

There is still potential left to improve the device. In particular the free space coupling between the waveguide end-facet and the PMF of the cWDM coupler can be replaced by a direct waveguide-fiber coupling to reduce the losses and to improve the compactness of the device. The well matched sizes of Ti-indiffused waveguide modes and fiber modes should allow an efficient coupling with significantly reduced losses. Additionally, the cWDM fiber coupler might be replaced by a dense WDM-fiber demultiplexer to narrow the transmission band and, thus, improve the indistinguishabilty of photon pairs generated by the two processes. Finally, a completely fiber pigtailed version seems to be feasible providing high quality entangled photon pairs from a versatile “Plug&Play” source.

Acknowlegdment

We thank Raimund Ricken and Viktor Quiring for the waveguide fabrication and Dr. Andreas Christ for many helpful discussions. We acknowledge the funding of parts of this work by the European Space Agency (ESA).

#194865 - $15.00 USD Received 29 Jul 2013; revised 20 Sep 2013; accepted 21 Sep 2013; published 7 Nov 2013